

Friction measurement in zero and adverse pressure gradient boundary layer using oil droplet interferometric method

Guy Pailhas · P. Barricau · Y. Touvet ·
L. Perret

Received: 26 June 2008 / Revised: 17 December 2008 / Accepted: 19 March 2009 / Published online: 5 April 2009
© Springer-Verlag 2009

Abstract The oil droplet interferometric technique has been used to investigate the skin friction distribution along a zero and adverse pressure gradient boundary layer developing in the Laboratoire de Mécanique de Lille wind tunnel. This experimental task was a part of the WALL-TURB project, funded by the European Community, in order to bring significant progress in the understanding of near wall turbulence in boundary layers. Skin friction values close to 0.01 Pa have been measured with this optical method. A comparison with the results obtained with hot-wire anemometry and macro-PIV demonstrates the great potential of the oil droplet technique.

1 Introduction

It is well known that the main turbulent events occur in the inner part of the boundary layer. Turbulence modelers have had always a great need for turbulence data in this region more particularly when the flow is separated or close to separation. Moreover, the knowledge of the wall shear stress remains fundamental for validation of computational

approaches. Until now, an accurate measurement of the skin friction distribution on a surface of aerodynamic interest can be considered as a difficult and crucial task in spite of the amount of developed skin friction measurement techniques. Most of them suffer from several shortcomings because they are based upon analogical laws or because they assume the universality of the logarithmic law, which is questionable. Methods that do not require any assumption about the form of the velocity profile, namely the nature of the flow close to the wall, should be favoured. This statement is true for the oil film interferometric method which is available for the direct and absolute skin friction measurement.

First techniques for measuring skin friction by depositing an oil film on the surface of an airfoil have been introduced over the past 30 years. From the concepts of Squire (1961) relating to the thin oil film equation, Tanner and Blows (1976) were the first to use the oil film interferometry concept. They quantified the thinning rate of the oil, measuring the variation in time of the oil thickness by lighting it with a laser beam. With the measurement of the oil thickness at many times, they determined the local skin friction using the oil film equation. About 10 years later, the technique took a new flight; from the technique developed by Tanner and Blows, Monson and Mater (1993) demonstrated that only a two-dimensional image of the interference pattern captured at the end of the wind tunnel run by illuminating the oil film with an extended light source was sufficient to determine the skin friction. Even now, the oil film technique did not only concern the research but also the industrial wind tunnels. In United States, Driver (1997) performed skin friction measurements in NASA Ames wind tunnel. Although the feasibility of the single image approach was demonstrated, the technique based upon the time dependence analysis of the

G. Pailhas (✉) · P. Barricau · Y. Touvet
Aerodynamics and Energetics Model Department,
ONERA/DMAE, 2 Av E. Belin, BP 74025,
31055 Toulouse, France
e-mail: guy.pailhas@onera.fr; guy.pailhas@onecert.fr

L. Perret
Laboratoire de Mécanique de Lille, UMR 8107,
59655 Villeneuve d'Ascq, France

Present Address:

L. Perret
Laboratoire de Mécanique des fluides, Ecole Centrale de Nantes,
1, rue Noë, 44300 Nantes, France

fringe pattern, from many images recorded at specified time intervals, provides accurate results and was commonly adopted. Maksimov et al. (1994) and Kornilov et al. (1992) used this technique in supersonic flows. Naughton and Brown (1996) developed a new interferometric method based upon the solution of the discretized form of the 2D oil film equation. They put into practice this method for complex flows where the skin friction does not remain constant in the main direction of the flow.

ONERA first focused its efforts on the oil film interferometric technique. This technique was at first validated in classical two-dimensional turbulent flows where the assumption of a monotonous evolution of the shear stress is admitted. This simplified hypothesis can no longer be retained when the flow is submitted to a strong adverse pressure gradient (APG). The interferometric method was consequently adapted for more complex flows before being used in the present experiment where very low skin friction values close to 0.01 Pa have been measured. Others direct measurement methods yield such high resolution as the technique proposed by Brücker et al. (2005) based upon the use of sensor film with arrays of hair-like flexible micro-pillars. These microcylinders must have precise cylindrical shape and aspect ratio since they strongly influence the sensitivity of the shear-stress measurement. Their manufacturing similar to the one of MEMS arrays remains expensive and meticulous. On the contrary, the oil droplet interferometric method does not require any manufacturing technique. The oil needs only to be calibrated in viscosity before being deposited on the tested surface. Additionally, in this method, the required experimental set-up is succinct and easily adaptable to any wind tunnel or experimental system. Moreover, the droplet technique enables measurements over extensive regions of the investigated model that must not occult some weaknesses of this technique due to its sensitivity to the tested surface quality, the vibration of the model or the optical system and the dust contamination.

2 Oil film interferometric method

This method is based upon the relationship between the thinning with time of an oil film deposited on the test surface exposed to the flow and the local wall shear stress. The governing differential equation that describes the slow viscous motion of a thin oil sheet is given by:

$$\frac{\partial h}{\partial t} + \frac{\partial}{\partial x} \left\{ \tau_x \frac{h^2}{2\mu} + \left[-\frac{\partial p_e}{\partial x} + \rho g_y \frac{\partial h}{\partial x} + \rho g_x \right] \frac{h^3}{3\mu} \right\} + \frac{\partial}{\partial z} \left\{ \tau_z \frac{h^2}{2\mu} + \left[-\frac{\partial p_e}{\partial z} + \rho g_y \frac{\partial h}{\partial z} + \rho g_z \right] \frac{h^3}{3\mu} \right\} = 0 \tag{1}$$

where $h(x, z, t)$ is the height of the oil film, ρ and μ the oil density and dynamic viscosity, respectively, g_x , g_y and g_z are the components of gravity in the x - y - and z -directions, τ_x and τ_z are the wall shear-stress components generated by the flow submitted to a pressure distribution $p_e(x, z)$.

The above equation provides the condition for which the transverse flow due to gravity is negligible with respect to the flow due to the wall shear stress, namely:

$$\tau_x \gg \rho gh$$

Generally this condition is verified.

Assuming the flow is two-dimensional and the external pressure field quite uniform, Eq. 1 can be further simplified as:

$$-\mu \frac{\partial h}{\partial t} = \frac{\tau_x}{2} \frac{\partial h^2}{\partial x} \tag{2}$$

If the wall friction depends upon x , it can be demonstrated (Brown and Naughton 1999) that the self similar solution of 2 is:

$$h(x, t) = \frac{\mu}{\sqrt{\tau_x(x)t}} \int_{x_0}^x \frac{dx}{\sqrt{\tau_x(x)}} \tag{3}$$

With the assumption that the shear-stress gradient in the x direction is negligible, relation 3 reduces to:

$$h(x, t) = \frac{\mu_0 x}{\tau_x t} \tag{4}$$

Inverting relation 3 provides the wall friction field from the measurement of the oil film height. Equation 1 can also be rewritten in discretized form and rearranged to be numerically solved for wall shear stress distribution (Naughton and Sheplak 2002).

The oil film thickness variation can be measured using interferometric technique. One part of the illuminating light is partially reflected by the air/oil interface (Fig. 1) whereas the remaining part passes through the film, is reflected by the solid surface and then travels back again through the film. These two parts of light (ψ_1 and ψ_2) interfere together and produce a fringe pattern, the separating distance of which is directly connected to the oil film height.

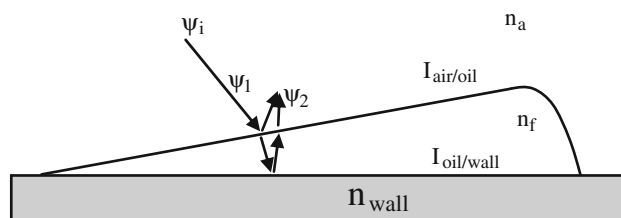


Fig. 1 Generation of the interferometric pattern close to the oil film

The intensity of the resulting wave ($\psi_1 + \psi_2$) is given by the interference formula:

$$I = I_1 + I_2 + 2\sqrt{I_1 I_2} \cos(\phi) \tag{5}$$

where I_1 and I_2 represent the intensity of the two interfering waves and ϕ the phase difference between ψ_1 and ψ_2 . Using basic interference optic formulas, it can be demonstrated that the height of the oil film is related to the phase difference ϕ of the light intensity signal obtained from the fringe pattern between the leading edge of the film and a local X station by the following relation:

$$h = \frac{\lambda\phi}{4\pi n_f^2 - n_a^2 \sin^2(\theta_i)} \tag{6}$$

where λ is the light wavelength, n_f and n_a , respectively, represent the refractive index of oil and air and θ_i the incidence angle of the light. Thus, if we are able to calculate the phase difference ϕ at any X stations in the fringe pattern, we are able to determine the thickness of the oil film at these considered X locations. Drawing inspiration from the work of Naughton and Brown (1996), ONERA/DMAE developed a data reduction algorithm based upon the Hilbert transformation (HT) of the recorded light signal. The HT of the signal $I(x)$ is the convolution of the original signal with $1/\pi x$. In the Fourier domain, the convolution can be written:

$$\tilde{I}_f(x) = H[I_f(x)] \tag{7}$$

$$\tilde{I}_f(x) = F^{-1}[F(1/\pi x) * F(I_f(x))] \tag{8}$$

where H and F represent the Hilbert and Fourier transformations, respectively. The local phase at each pixel in the interferogram can be extracted from:

$$\phi = \tan^{-1}(\tilde{I}_f(x)/I_f(x)) \tag{9}$$

Then, the total phase Φ_t (corresponding to the signal phase difference from the leading edge of the film to the local X station) can be calculated. Once the total phase Φ_t is known, the height of the oil film at each corresponding pixel can be calculated using relation 6.

Though this technique was validated in the case of a classic ZPG two-dimensional turbulent boundary layer, it presents some drawbacks in the case of more complex flows. The phase determination using the Hilbert transformation can be questionable. In separated or recirculating flow region, the friction vector may exhibit a sign reversal. In fact, we make the assumption that the oil film thickness increases in a monotonous way from the leading edge of the film; this hypothesis is not at all realistic when the flow is submitted to a strong wall friction gradient. Let us consider a given friction distribution (Fig. 2). This friction distribution gives from relation 3 two oil film height evolutions (Fig. 3) for two different times.

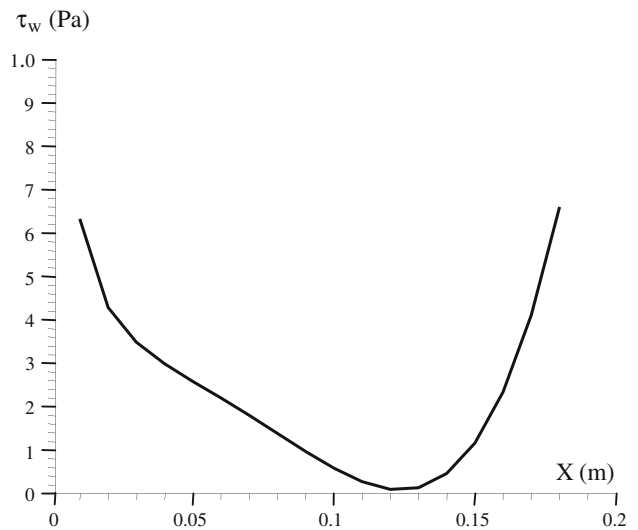


Fig. 2 Starting skin friction distribution

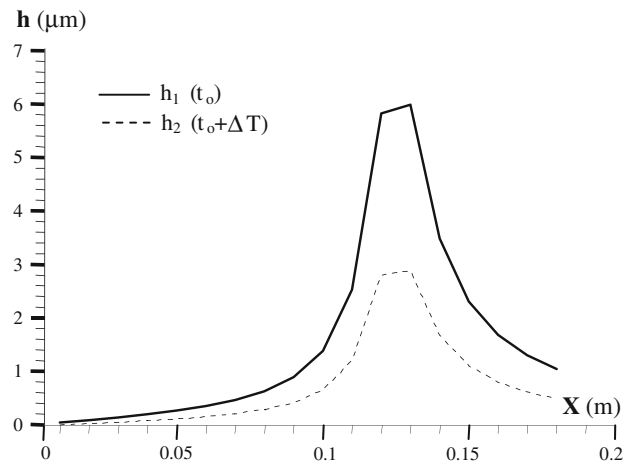


Fig. 3 Oil film profiles derived from skin friction distribution

From these oil film thickness evolutions, we can simulate a “theoretical” $I(x)$ intensity profile as indicated in Fig. 4.

By applying the Hilbert transform on the previous simulated intensity profile, we obtain the monotonous h profile (Fig. 5) in disagreement with the real h evolution; the sign reversal occurring on the slope of the oil film height curve cannot be detected with the Hilbert transformation.

From this point, a veering of the computed τ_p distribution with respect to the real skin friction distribution can be noticed (Fig. 6). The sudden skin friction variations occurring for a boundary layer submitted to a strong pressure gradient cannot be reproduced.

As a result a new implementation of the interferometric method was required.

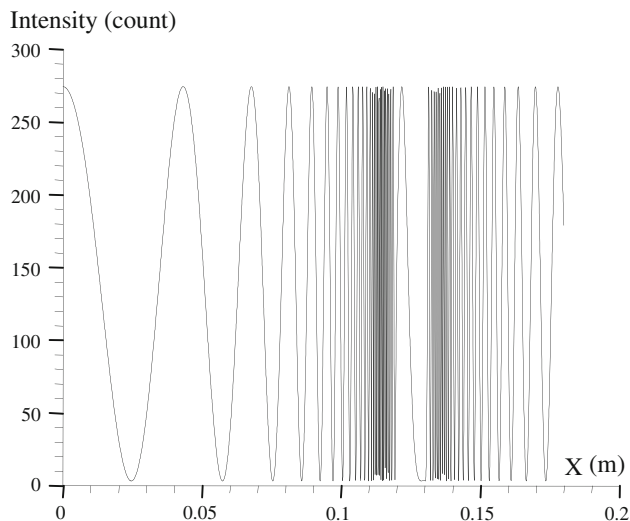


Fig. 4 Intensity profile derived from h_1 profile

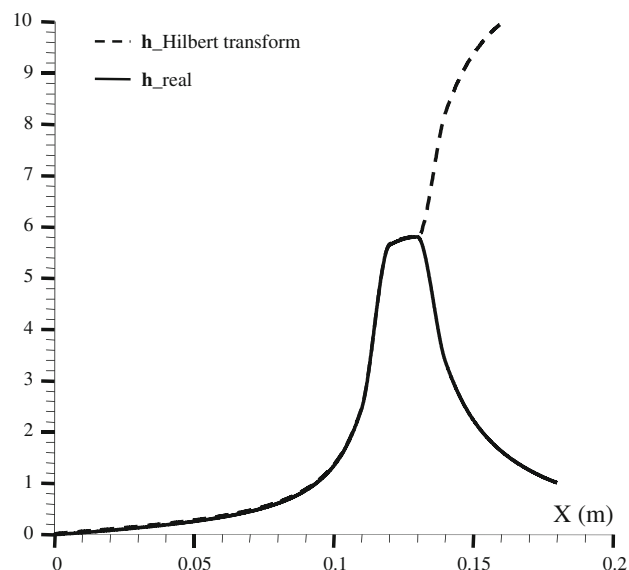


Fig. 5 Oil film profiles

3 Oil droplet interferometric method

An alternative approach for measuring skin friction in high wall shear gradient region consists in applying small oil droplets (Ruedi et al. 2003), in order to cut out this region in small area elements over which the wall shear stress can be considered as constant, providing interferometric patterns with a constant step interfringe. This method which consists in depositing an oil droplet on the test surface and viewing it with a long focal length optical system was used in the present experiments.

The fringe spacing or interfringe is given by the following formula:

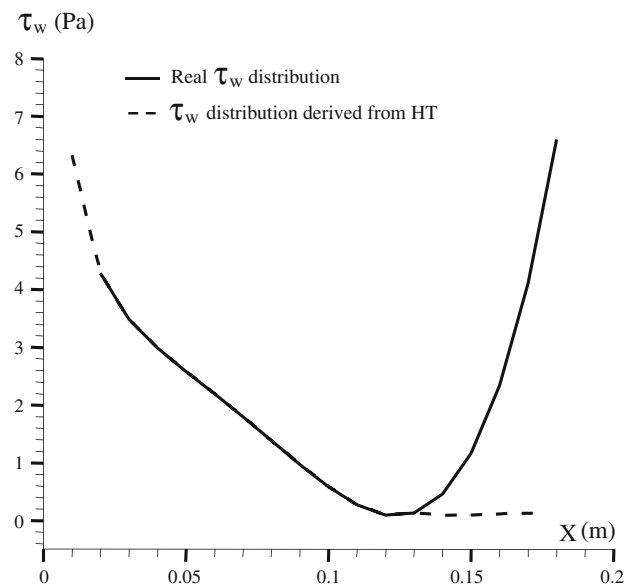


Fig. 6 τ_w distribution

$$\text{Int} = \frac{\lambda x}{2n_0 h} \quad (10)$$

The replacement of h by its expression 4 in the above relation leads to the following formula for the wall shear stress:

$$\tau_w = \frac{2n_0 \mu_0 c a}{\lambda} \quad (11)$$

where c is the calibration coefficient (mm/pixel) and a the slope of the interfringe versus time curve (pixels/s). For three-dimensional flows, the processing programme based upon the rotation of a grid over the fringes pattern allows the selection of a line normal to the fringes to determine the wall friction direction. That way, both the modulus and the direction of the wall shear stress can be determined. The interfringe is extracted from the Fourier transformation applied to the intensity levels provided by the interferometric pattern. By weighting this signal by a Laplace-Gauss window and detecting the position of the characteristic peak in the Fourier space with a least square method in order to find the best Gaussian fit of this local peak, the interfringe value can be estimated with sub-pixel accuracy.

Once the interfringe is calculated for each interferometric pattern acquired during the run, the curve describing the fringe spacing versus time can be plotted (Fig. 7).

Then the slope of the best fitted straight line, obtained with a least square method, is calculated to extract the skin friction value τ_w according to formula 11, provided that the oil characteristics and the optical calibration coefficient are known.

Every sequence of interferometric images was recorded at a fixed acquisition period (8 s), with a definition of

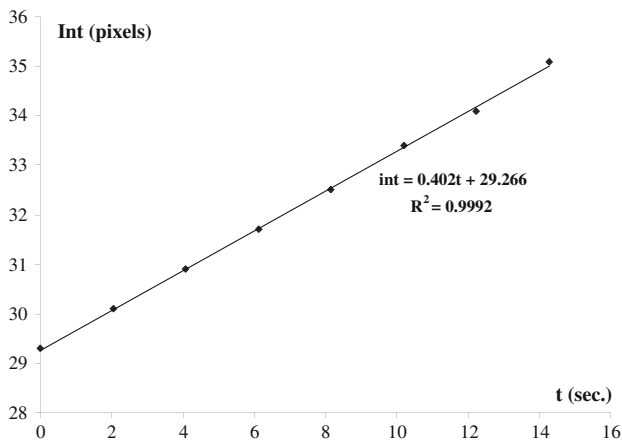


Fig. 7 Fringe spacing versus time

1,280 × 1,024 pixels and stored as bitmap files. An example of interferometric images obtained in the present experiment, covering a field of view of 7.7 × 6.2 mm², is given in Fig. 8.

4 Oil

The oil droplet spreads more or less quickly depending on the skin friction level and the oil viscosity. In order to obtain a rather good fringe visibility on the interferograms and to satisfy the Shannon sampling criterion, it is necessary to keep the interfringe value varying between 20 and 200 pixel values during the acquisition step. The choice of the oil viscosity depends upon the transitory time after which the flow is stabilized, the tunnel run time, the temperature of the flow and the magnitude of the wall friction to be measured. From the knowledge of the Laboratoire de Mécanique de Lille (LML) experimental conditions, preliminary experiments were carried out at ONERA in a fully developed flow in a rectangular duct to define the range of

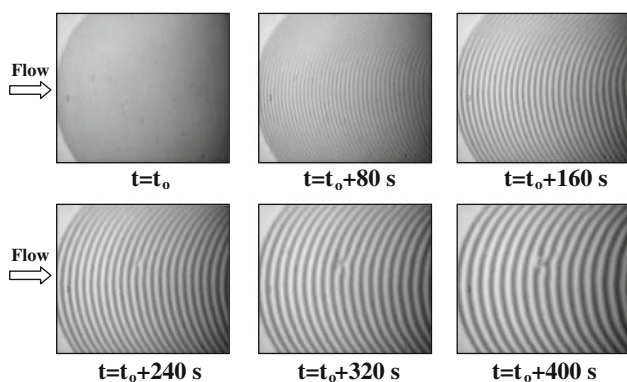


Fig. 8 Example of fringe patterns captured during the tests

viscosity and to test the behaviour of some low viscosity oils. These experiments brought out that an oil of viscosity below 10 cSt was not well adapted to the skin friction measurement. The spreading of the oil limits its use in the case of low viscosity. The radius $R(t)$ of an oil droplet is proportional to $(t/\nu)^{1/8}$; so, the lower the viscosity, the greater the spreading is. Three Dow Corning silicon oils of 10, 20 and 50 cSt were selected for LML.

The manufacturer gives the viscosity of each oil sample for a standard temperature of 25°C, with an uncertainty of ±5%. Given that the oil viscosity is the largest source of error in skin friction measurements (see Sect. 10 below), it was necessary to accurately calibrate the selected oils. These calibrations were carried out independently at LML with a Couette viscometer and at ONERA with a capillary viscometer, respectively. The oil temperature had to be carefully monitored during the viscosity measurements. A comparison of the two calibrations is given in Figs. 9, 10, and 11 where the evolution of the dynamic viscosity is plotted as a function of the temperature. The measurement uncertainty was estimated at ±1% for each of the two calibration methods. The error bars represent the uncertainty level according to a 95% confidence interval. The LML and ONERA calibrations are in perfect agreement for the 20 cSt viscosity oil. The error bars of each calibration curve overriding each other for the 50 cSt oil, the mean viscosity between the two calibrations may be considered as the correct one. The deviation between the two calibration curves for the 10 cSt oil was questionable. Complementary calibration tests evidenced that the Couette viscometer was pushed beyond its limits to measure the lowest viscosity.

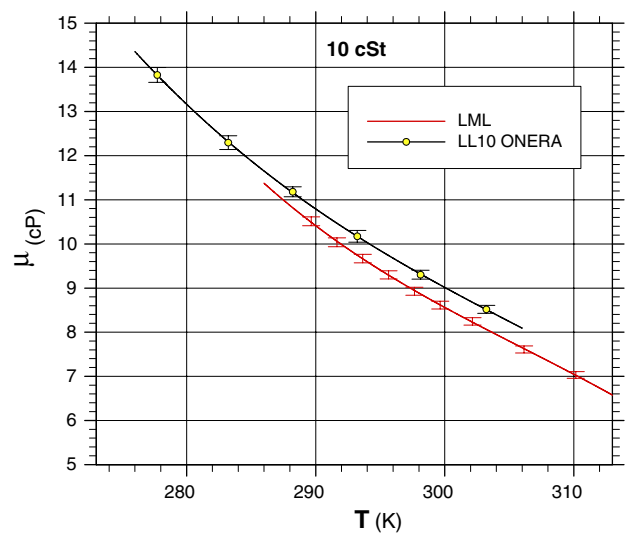


Fig. 9 Oil viscosity calibration (10 cSt)

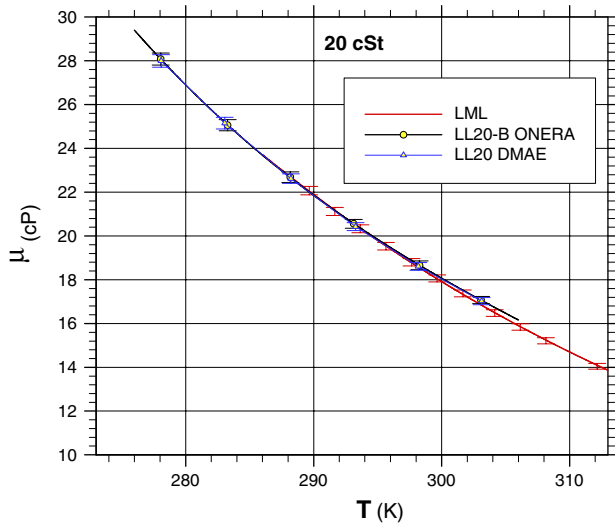


Fig. 10 Oil viscosity calibration (20 cSt)

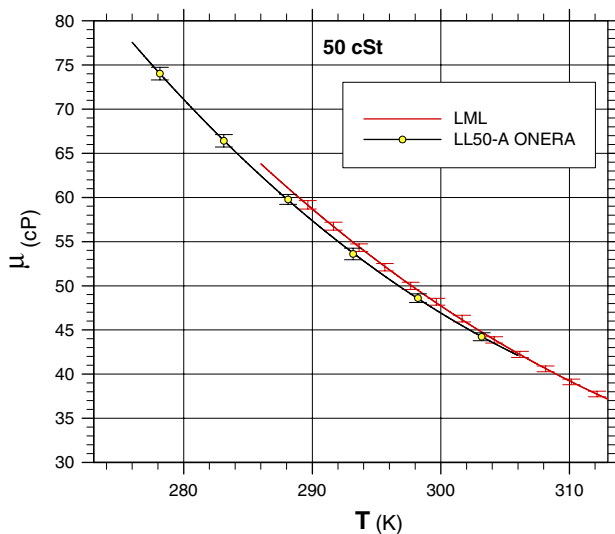


Fig. 11 Oil viscosity calibration (50 cSt)

5 Test surface

The interferometric method imposes constraints upon the surface on which the oil droplet is deposited. First of all, the surface must be perfectly flattened, without any roughness in order to prevent the apparition of chevron-patterned interferograms (Fig. 12).

Furthermore, the interferometric method requires that the surface has the adequate reflection properties. It is mostly necessary to add a specific material on the test surface in order to enhance the fringe contrasts, defined by:

$$C = \frac{I_{\max} - I_{\min}}{I_{\min} + I_{\max}} = \frac{2\sqrt{I_1 I_2}}{I_1 + I_2} \tag{12}$$

where I_1 and I_2 represent the intensity of the two interfering waves (Fig. 1). By introducing the coefficient of reflection

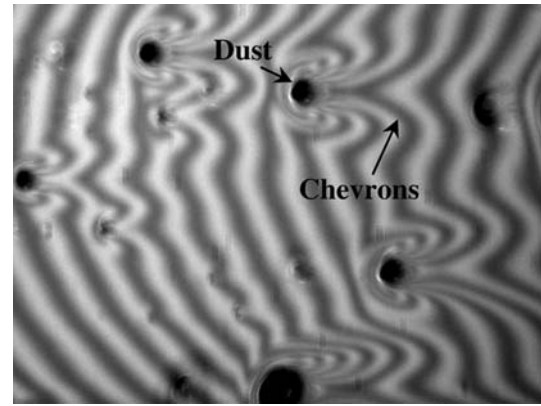


Fig. 12 Example of chevron-patterned interferogram produced by dusts

for the two concerning interfaces ($R_{\text{air/oil}}$ and $R_{\text{oil/wall}}$), we can write:

$$I_1 = R_{\text{air/oil}} I_i \text{ and } I_2 = (1 - R_{\text{air/oil}})^2 R_{\text{oil/wall}} I_i \tag{13}$$

with:

$$R_{\text{air/oil}} = \left(\frac{n_{\text{air}} - n_{\text{oil}}}{n_{\text{air}} + n_{\text{oil}}} \right)^2 \text{ and } R_{\text{oil/wall}} = \left(\frac{n_{\text{wall}} - n_{\text{oil}}}{n_{\text{wall}} + n_{\text{oil}}} \right)^2 \tag{14}$$

Finally, we obtain:

$$C = \frac{I_{\max} - I_{\min}}{I_{\min} + I_{\max}} = \frac{2\sqrt{I_1 I_2}}{I_1 + I_2} = \frac{2(1 - R_{\text{air/oil}}) \sqrt{R_{\text{air/oil}} R_{\text{oil/wall}}}}{R_{\text{air/oil}} + R_{\text{oil/wall}} (1 - R_{\text{air/oil}})^2} \tag{15}$$

The characteristics of various test surfaces are given in Table 1, assuming $n_{\text{air}} = 1$ and $n_{\text{oil}} = 1.4$.

6 Experimental test facility

This experimental study was conducted in the framework of the WALLTURB European project the global aim of which being to bring a significant progress in the understanding and modelling of near wall turbulence in boundary layers. This goes particularly through a precise skin friction measurement as undertaken in the present experimental study.

Table 1 Test surface characteristics

Test surface (wall)	n_{wall}	$R_{\text{air-oil}}$	$R_{\text{oil-wall}}$	C
Polished stainless steel	∞	0.03	1	0.33
Mylar	1.67	0.03	0.01	0.81
Glass and plexiglass	1.5	0.03	0.001	0.39

The experiments were carried out in the Laboratoire de Mécanique de Lille boundary layer wind tunnel. The boundary layer developing on the floor of the 15 m long channel, enters a 5 m long test section ($2 \times 1 \text{ m}^2$, $w \times h$) equipped with glass panels. The maximum external velocity (10 ms^{-1}) allows Reynolds numbers Re_θ based upon the momentum thickness between 7.5×10^3 and 2×10^4 to be obtained. The wind tunnel velocity and temperature are kept constant with accuracies respectively better than 1% and 0.2°C during time periods of 8 h.

The pressure gradient undergone by the boundary layer in the upstream 15 m of the channel is very small ($-0.53 \text{ Pa}\cdot\text{m}^{-1}$ at 10 ms^{-1}). Thus, ZPG conditions are nearly achieved in the test section. To analyze the boundary layer submitted to a significant APG a bump was mounted onto the test section floor. This bump (Fig. 13) has a maximum height of 0.33 m and a length of 3.40 m (Bernard et al. 2003).

The shape of the bump has been computed to avoid separation and to generate an APG representative of an airfoil at a high angle of attack (Fig. 14). The computed shape factor reaches a maximum value of 1.66 at the end of the bump ($X = 18.70 \text{ m}$), which is characteristic of a strongly destabilized boundary layer.

7 Experimental set-up

To measure the local wall shear stress, the oil droplet interferometric technique was applied. For this purpose, the optical setup shown in Fig. 15 was installed around the test section of the wind tunnel.

The oil droplet deposited on the surface was illuminated by a halogen lamp. The interference pattern was captured by a digital CCD camera (Lavision sensicam $1,280 \times 1,024$ pixels) initially dedicated to PIV measurements. An optical line filter ($\lambda = 590 \text{ nm}$, FWHM = 3 nm) was mounted in front of the camera sensor to filter



Fig. 13 Bump on the test section floor

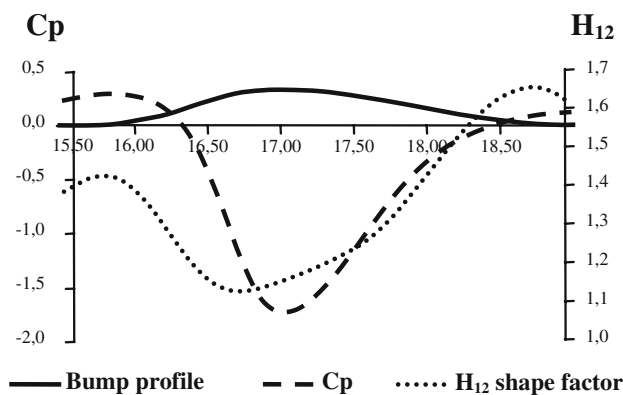


Fig. 14 Bump profile, computed pressure coefficient and boundary layer shape factor H_{12} as a function of the longitudinal location (Dassault computations)

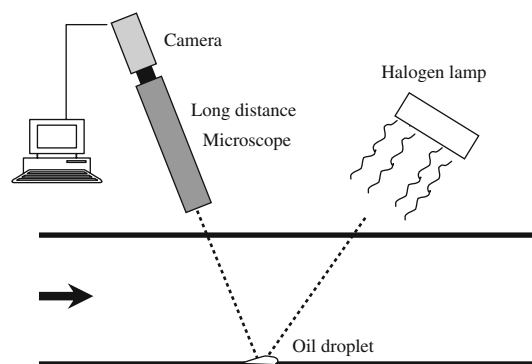


Fig. 15 Optical setup

the white illuminating light. The camera was fitted with a long distance microscope objective (Questar QM1) featured by a working range of 560–1,520 mm. This optical system and the lamp were mounted on a traversing mechanism (Fig. 16) located on the test section ceiling. The distance between the microscope and the oil droplet was about 1,200 mm. At this working distance, the camera and its long distance microscope provide a field of view of about $8 \times 6 \text{ mm}^2$.

The interferograms were digitized by the CCD camera; then, they were transferred to a personal computer before being analyzed with a home made algorithm developed by ONERA in order to extract the local skin friction value.

To enhance the fringe pattern produced, glass panel and Mylar film were used as test surfaces. A glass-made insert (Fig. 17) was moved from one test section floor measurement station to another for ZPG experiment. APG measurements were performed on a black paint-backed Mylar film of $1.5 \times 1.5 \text{ cm}^2$ glued onto the bump surface (Fig. 18). The Mylar stamp was placed in the measurement area in such a manner that the desired measurement location is approximately on its centre. The glass insert was

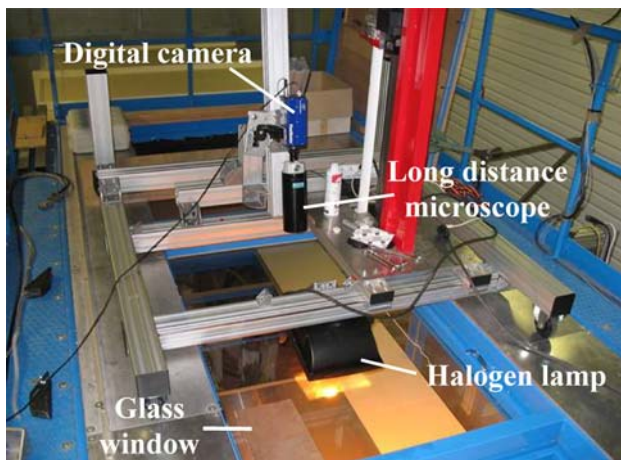


Fig. 16 Traversing mechanism

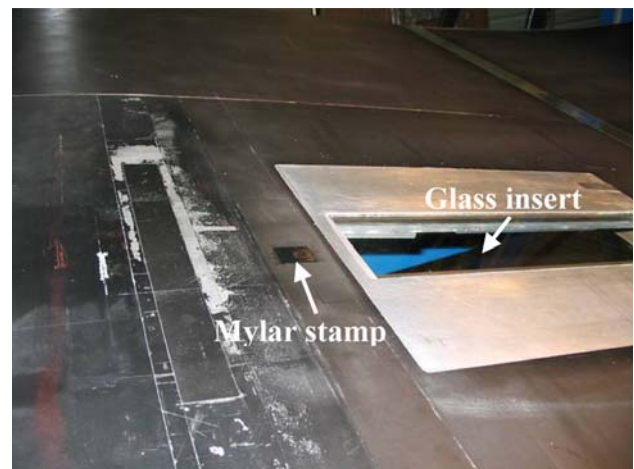


Fig. 18 Mylar stamp and glass surface mounted on the test bump

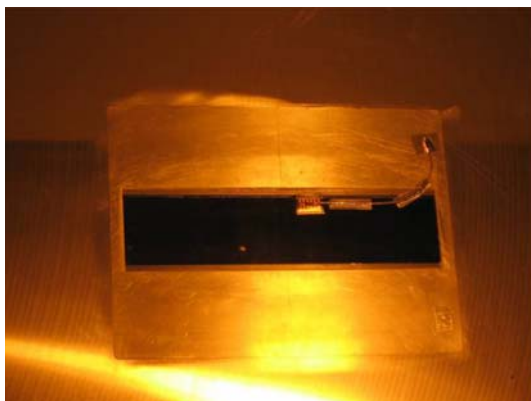


Fig. 17 Glass insert surface

also used as support surface in the rear constant slope region of the bump (Fig. 18).

8 Experimental operating mode

The oil film interferometric method requires that the thermal gradient in the test section flow as well as on the test surface is insignificant. Thus, for each test the wind tunnel was started long time before in order to stabilize the temperature of the flow and also of the tested wall. Then, the test section was opened and the oil droplet deposited on the glass insert or on the Mylar stamp previously glued on the bump. An individual drop was placed on the test surface using a glass rod with a round tip. At most, one minute was needed to start the wind tunnel up again at the fixed reference velocity. During the experiment, the temperature of the air and the temperature of the test surface were permanently monitored by the use of thermocouples both installed in the air circuit and onto the test surface. A difference of 2°C between the flow and the model surface was

generally noticed. Nevertheless, the air temperature remained constant during the measurement test whereas the model temperature fluctuated by 0.2°C. As soon as the fringe pattern took form on the screen, the image recording was launched. According to the oil spreading time (connected to the reference velocity) 50 or 100 images were recorded at 8 s timing period, corresponding to an acquisition duration varying from 400 to 800 s. After this period, the interfringe became too large, compared to the CCD size, to be correctly extracted.

9 ZPG experiment

The first test campaign was devoted to the measurement of the wall shear stress in a zero pressure gradient boundary layer. Friction measurements were carried out at two streamwise locations $X = 18$ m and $X = 19.6$ m from the entrance of the wind tunnel where the characteristics of the turbulent boundary layer were known from hot wire experiments. ZPG experiments were conducted at four external velocities U_0 : 3, 5, 7, 10 ms^{-1} . A set of only two different oil viscosities (20 and 10 cSt) were used. The 10 cSt oil was chosen for the measurement of the lower wall friction corresponding to the reference velocity of 3 ms^{-1} . The ZPG test conditions are summed up in Fig. 19.

Experiments for a fixed streamwise location and a given reference velocity were performed twice or three times to be sure of the validity and the repeatability of the measurement.

All the measurements were performed on the glass test surface. Table 2 lists the values of the mean skin friction obtained from the data reduction analysis for the experiments conducted at the four fixed reference velocities 3, 5, 7 and 10 ms^{-1} . The uncertainties calculated from

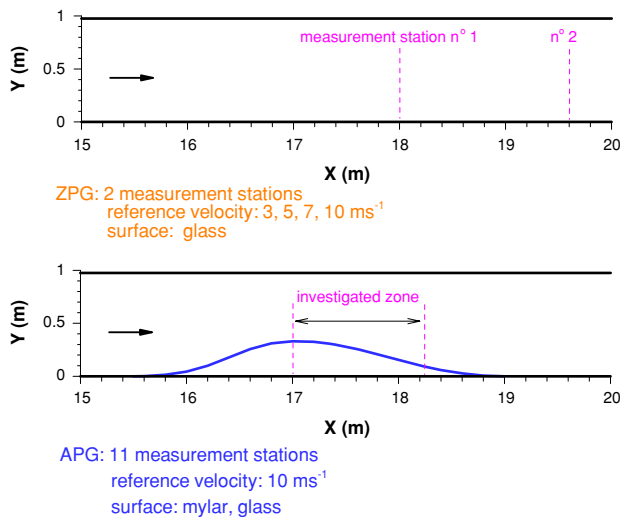


Fig. 19 ZPG and APG test conditions

Table 2 Mean skin friction measurements (ZPG case)

X = 19.6 m				
U_0 (ms ⁻¹)	3	5	7	10
ν_{oil} (cSt)	10	20	20	20
τ_w (Pa)	0.015	0.042	0.081	0.147
	0.018	0.042	0.074	0.151
Deviation (%)	20.00	0.00	8.64	7.48
X = 18.0 m				
U_0 (ms ⁻¹)	3	5	7	10
ν_{oil} (cSt)	10	20	20	20
τ_w (Pa)	0.016	0.040	0.076	0.164
	0.016	0.042	0.079	0.155
	0.016	0.039	0.082	0.137
Deviation (%)	0	7.69	7.89	19.71

measurements series repeated at least three times with an occurrence probability of 95% are also reported.

The measurement repeatability at the upstream location for the lower reference velocity is noteworthy. Vibrations of the optical set-up located on the roof of the wind tunnel were observed during the experiments at the higher reference velocity ($U_0 = 10 \text{ ms}^{-1}$); they have contributed to increase the noise level in the interference pictures. Consequently, the skin friction computation became less reliable as indicated by the corresponding relatively high deviation values. The evolution of the mean skin friction versus the reference velocity is also plotted in Fig. 20 for the two longitudinal stations.

To characterize the basic flow, hot-wire anemometry was mainly used (Carlier and Stanislas 2005). Table 3 gives the global parameters deduced from the measured

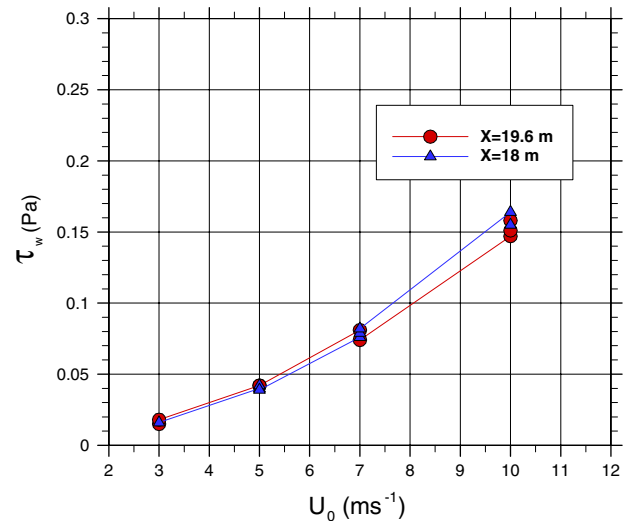


Fig. 20 Mean skin friction measurements (ZPG)

velocity profiles as a function of the abscissa X and the reference external velocity U_e . From these experiments, the wall shear stress through the friction velocity u^*_{C}

$$\tau_w = \rho u^*_{C^2}$$

and consequently the friction coefficient Cf_C

$$Cf_C = 2 \left(\frac{u^*_{C}}{U_e} \right)^2$$

are deduced from a Clauser plot, supposing that the von Karman constant is $\kappa = 0.41$.

Stereoscopic PIV measurements were also undertaken at $X = 19.6 \text{ m}$ in the fully turbulent boundary layer developing on the test section floor. The PIV interrogation procedure is detailed in (Foucaut et al. 2006). The maps are stored and post-processed with a LML software. From this analysis the wall shear stress was evaluated and the corresponding friction velocity u^*_{PIV} and friction coefficient Cf_{PIV} are given in Table 3. The friction velocity u^*_{int} relating to oil film interferometric method is also reminded in Table 3.

The skin friction coefficient measured at $X = 19.6 \text{ m}$ by the three above-mentioned methods are compared in Fig. 21 varying the reference velocity from 3 to 10 ms⁻¹. Also plotted in Fig. 21 is the Fernholz correlation (1996) providing a simple relation between the skin friction coefficient and the Reynolds number in ZPG flows. As can be seen, the agreement is quite good between the three measurement methods for the three reference velocities 5, 7 and 10 ms⁻¹; Cf deviation does not exceed 4%. At the lower reference velocity ($U_0 = 3 \text{ ms}^{-1}$) for which the wall shear stress τ_w is close to 0.02 Pa deviations between PIV and interferometry and between PIV and hot-wire anemometry are 3.5 and 7%, respectively. If we refer to Fernholz law, it can be seen that the three measurement

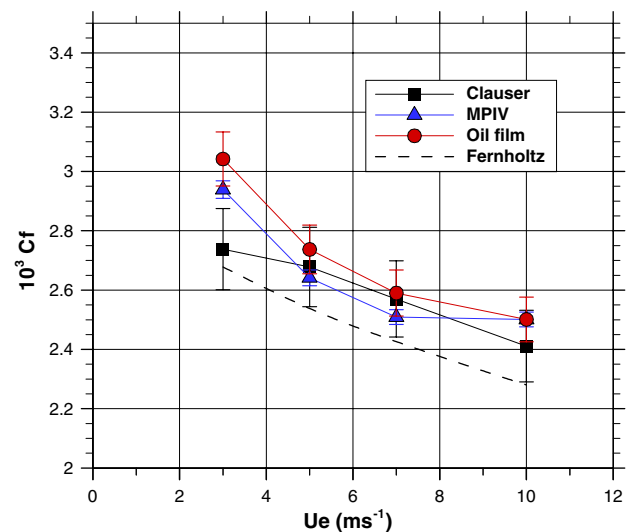
Table 3 Global parameters of the boundary layer (ZPG case)

R_θ	8,200	11,500	14,500	21,000
$X = 19.6$ m				
dP/dx (Pa/m)	-0.065	-0.151	-0.247	-0.528
U_e (m/s)	3.0	5.0	7.0	10.0
δ (m)	0.350	0.319	0.298	0.304
R_δ	69,918	106,925	139,497	202,588
δ_1 (m)	0.0551	0.0443	0.0396	0.0398
θ (m)	0.0409	0.0342	0.0309	0.0312
u^*_c (m/s)	0.111	0.184	0.252	0.3475
$10^3 Cf_c$	2.738	2.678	2.570	2.411
u^*_{PIV} (m/s)	0.115	0.1827	0.249	0.354
$10^3 Cf_{PIV}$	2.939	2.641	2.509	2.501
u^*_{int} (m/s)	0.117	0.186	0.253	0.354
$10^3 Cf_{int}$	3.042	2.737	2.590	2.501
R_θ	7,700	10,100	13,500	19,000
$X = 18.0$ m				
dP/dx (Pa/m)	-0.065	-0.151	-0.247	-0.528
U_e (m/s)	3.0	5.0	7.0	9.9
δ (m)	0.332	0.279	0.281	0.288
R_δ	70,085	97,087	136,887	194,921
δ_1 (m)	0.0482	0.0377	0.0350	0.0353
θ (m)	0.0362	0.0291	0.0276	0.0280
u^*_c (m/s)	0.112	0.185	0.255	0.350
$10^3 Cf_c$	2.788	2.738	2.654	2.450
u^*_{int} (m/s)	0.115	0.183	0.256	0.356
$f 10^3 Cf_{int}$	2.938	2.678	2.674	2.534

techniques provide an expected Cf evolution as function of the Reynolds number except at 3 ms^{-1} . Nevertheless, measured Cf values are stronger than the ones corresponding to ZPG flow whatever the measurement technique used because of a slight negative pressure gradient (B. Aupoix, private communication). The error bars corresponding to the estimated measurement uncertainty are also given in the Fig. 21. The uncertainty analysis relating to oil film measurements is detailed farther on.

10 APG experiment

A second test campaign was conducted to measure the wall shear stress distribution in an APG boundary layer configuration. Measurements were carried out at eleven streamwise locations from $X = 17$ m, corresponding to the top of the bump to $X = 18.24$ m in the rear part of the bump sloping region (Fig. 19). APG experiments were conducted at a fixed reference flow velocity of 10 ms^{-1} . Two different oil viscosities were used: 50 cSt in the top region of the bump (where the acceleration of the flow

**Fig. 21** Skin friction evolution w.r.t. Reynolds number at $X = 19.6$ m (ZPG)

ends) and 20 cSt elsewhere (in the decelerating region of the flow).

Table 4 collects the various repeated wall shear-stress (τ_{wint}) measurements at each investigated station along the second half part of the bump and indicates their corresponding deviation. The wall shear-stress (τ_{wC}) inferred from a Clauser plot of the velocity profiles obtained from hot-wire anemometry data is also given. These comparisons are referring to experiments formerly performed; unfortunately, no PIV shear-stress data in APG configuration were undertaken at this time.

Except for the top of the bump (from $X = 17$ to 17.10 m) where the pressure gradient exhibits a sign reversal, the repeatability of the wall shear-stress measurement is not far to be perfect. On the whole measurement tests were repeated at least three times; the mean uncertainty on τ_w is close to 3% with a 95% probability.

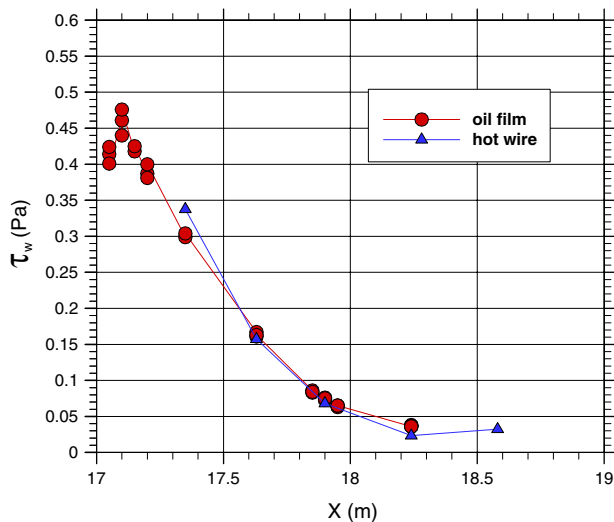
The evolution of the wall shear stress along X direction is given in Fig. 22. A comparison with the wall shear stress obtained from the Clauser technique using hot-wire anemometry data (Ruedi et al. 2003) is also given. The agreement between the two techniques is relatively good if the comparison at $X = 17.30$ m is not taken into account. However, a comparison performed all along the sloping region of the bump would evidence more precisely the intersection of the curves and consequently would indicate a deviation between the two measurement methods.

11 Uncertainty analysis

If we refer to relation 11, the accuracy of the wall shear-stress measurement depends upon the potential uncertainties in the valuation of:

Table 4 Mean skin friction measurements (APG)

X (m)	17.00	17.05	17.10	17.15	17.20	17.35	17.63	17.85	17.90	17.95	18.24
ν_{oil} (cSt)	50	50	50	50	50	20	20	20	20	20	20
τ_{wint} (Pa)	0.513	0.414	0.461	0.418	0.387	0.299	0.167	0.086	0.073	0.063	0.036
	0.474	0.424	0.440	0.425	0.381	0.304	0.161	0.083	0.076	0.065	0.038
		0.401	0.476		0.400		0.163	0.084	0.075	0.065	0.037
											0.036
Deviation (%)	8.23	5.74	8.18	1.67	4.99	1.67	3.73	3.61	4.11	3.17	5.56
τ_{wC} (Pa)						0.338	0.157		0.068		0.023

**Fig. 22** Mean skin friction measurements (APG case)

- the oil viscosity,
- the calibration coefficient,
- the fringe spacing through the fitting of the interfringe versus time curve,
- the optical characteristics of the oil (n_0),
- the emitted light wavelength (λ).

11.1 Oil viscosity

The uncertainty in the determination of the oil cinematic viscosity was estimated as $\pm 1\%$. The oil manufacturer provides the specific density with an uncertainty of $\pm 0.4\%$ that leads to a dynamic viscosity uncertainty of $\pm 1.4\%$.

11.2 Calibration coefficient

The uncertainty in the physical location of the pixels in the image brings out a calibration error close to $\pm 0.5\%$.

11.3 Fringe spacing

To analyze the uncertainty attached to the fringe spacing evaluation, synthetic interferometric images with perfectly

controlled interfringe value, contrast and noise level have been created as input data file for the home made software. The higher fringe standard deviation (0.12 pixel) related to a 50 pixels size interfringe, leads to an uncertainty in the fringe spacing evaluation of 0.24%.

11.4 Slope of the interfringe versus time curve

The data reduction algorithm provides the time evolution of the fringe spacing along a line defined by the operator as aligned with the mean flow direction. The slope of interfringe versus time curve is then calculated by a least square method. The cumulated uncertainty results in the fringe digitization and fitting error effects. In previous works, it was estimated that the fitting error was around $\pm 0.2\%$.

11.5 Oil index of refraction

From information given by the manufacturer on the oil characteristics for a standard temperature of 25°C, it is possible to calculate a specific index of refraction which is hardly dependent upon the pressure and the temperature. So, the uncertainty on the oil index of refraction was evaluated as $\pm 0.16\%$.

11.6 Light wavelength

The oil droplet must be lighted with a “white” light passing through an optical band pass filter. The incidence angle of the light and the temperature variation of the ambient environment affect the characteristics of the filter. Consequently, the present experimental conditions lead to a light wavelength uncertainty of $\pm 0.5\%$.

Finally, the above analysis indicates that the shear stress can be measured with an uncertainty of $\pm 3\%$.

12 Measurement reproducibility

The dispersion of the results provided by the oil film interferometry technique, particularly in the immediate

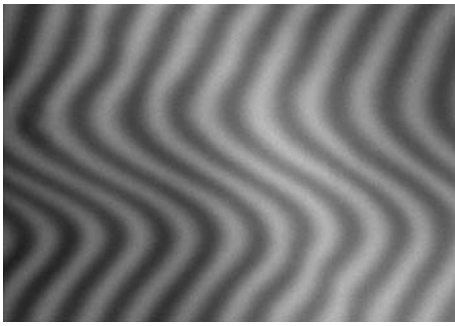


Fig. 23 Undulations observed in the fringe pattern at $X = 17$ m station

vicinity of the top of the bump (APG case), is greater than the estimated uncertainty (Table 4). This dispersion can be related to the spatial undulations observed in the fringe pattern acquired by the CCD camera during these tests. Fig. 23 gives an example of this phenomenon observed at the $X = 17$ m station.

These undulations might be closely linked to the deformation of the Mylar stamp which might be not perfectly flattened onto the test surface. Moreover, this deformation can fluctuate during the run due to the stress produced by the flow. Therefore, the uncertainty attached to the fringe spacing evaluation is deeply increased and consequently, deviations on skin friction values occur.

13 Conclusion

In this experiment, the oil droplet method which is an alternative approach to the classical oil film interferometric method has been used to measure the skin friction in a flow submitted to zero and strong APG. In this approach, the region of high shear gradient is cut in small areas in such a way that the shear stress can be locally considered as constant. The present experimental study demonstrated that this technique can be used for the measurement of very weak skin friction values, even in a strongly destabilized boundary layer. The low deviation between the various repeated measurements at the end of the sloping region of the bump, where the magnitude of the shear stress is close to zero, is a significant result. The overall measurement uncertainty is estimated at about 3% with a 95% confidence interval. This is quite good compared to other measurement techniques and quite interesting for the bump test case. The agreement between the results obtained from oil droplet and hot-wire anemometry seems to be satisfactory. Nevertheless, the intersection of the curves corresponding to the two measurement series indicates a difference in the measurement techniques. The oil droplet measurements at $X = 17.30$ m station (characterized by a quite good

reproductibility) are certainly much more reliable than the hot wire measurements inasmuch as the use of a universal logarithmic law to represent the recovery region of the velocity profile remains rather questionable in APG flow conditions. The relative good agreement between macro-PIV and interferometry in present ZPG flow experiment is an encouraging result. At last, the reliability of this promising technique in low skin friction measurement was confirmed in this experiment.

Acknowledgments This work has been performed under the WALLTURB project. WALLTURB (A European synergy for the assessment of wall turbulence) is a collaboration between LML UMR CNRS 8107, ONERA, LEA UMR CNRS 6609, LIMSI UPR CNRS 3251, Chalmers University of Technology, Ecole des Mines de Paris, CNRS groupe Instabilité et Turbulence Saclay, University of Cyprus, University of Rome la Sapienza, University of Surrey, Universidad Politécnica de Madrid, Technische Universität München, Czestochowa University of Technology, FFI, DASSAULT AVIATION, AIRBUS. The project is managed by LML UMR CNRS 8107 and is funded by the CEC under the 6th framework programme (CONTRACT N°: AST4-CT-2005-516008). The authors gratefully acknowledge the LML wind tunnel team and more specially Pr. M. Stanislas. Furthermore, we really appreciated fruitful discussions with Dr. B. Aupoix.

References

- Bernard A, Foucaut JM, Dupont P, Stanislas M (2003) Decelerating boundary layer: a new scaling and mixing length model. *AIAA J* 41(2):248–255
- Brown JL, Naughton JW (1999) The thin oil film equation. NASA/TM-208767
- Brücker CH, Spatz J, Schröder W (2005) Feasibility study of wall shear stress imaging using microstructured surfaces with flexible micropillars. *Exp Fluids* 39:464–474
- Carlier J, Stanislas M (2005) Experimental study of eddy structures in a turbulent boundary layer using particle image velocimetry. *J Fluids Mech* 553:143–188
- Driver DM (1997) Application of oil film interferometry skin friction to large wind tunnels. AGARD Conference Proceedings CP-201
- Fernholz HH, Finley PJ (1996) The incompressible zero-pressure-gradient turbulent boundary layer: an assessment of the data. *Prog Aerospace Sci* 32:245–311
- Foucaut JM, Kostas J, Stanislas M (2006) Wall shear stress measurement using stereoscopic PIV. 12th International symposium on flow visualization, Göttingen, Germany
- Kornilov I, Pavlov AA, Shpak SI (1992) On the techniques of skin friction measurement using optical method. International conference on the methods of aerophysical research, Novosibirsk
- Maksimov AI, Pavlov AA, Shevchenko AM (1994) Development of the optical skin friction measurement technique for supersonic flows. International conference on the methods of aerophysical research, Novosibirsk
- Monson DJ, Mateer G (1993) Boundary layer transition and global skin friction measurement with an oil fringe imaging technique. SAE Paper 932550
- Naughton JW, Brown JL (1996) Surface interferometric skin-friction measurement technique. 19th AIAA advanced measurement and ground testing technology conference, 17–20 June
- Naughton JW, Sheplak M (2002) Modern development in shear-stress measurement. *Prog Aerospace Sci* 38:515–570

- Ruedi JD, Nagib H, Osterlund J, Monkewitz PA (2003) Evaluation of three techniques for wall-shear measurements in three-dimensional flows. *Exp Fluids* 35:389–396
- Squire LC (1961) The motion of a thin oil sheet under the steady boundary layer on a body. *J Fluids Mech* 11:161–179
- Tanner LH, Blows LG (1976) A study of the motion of oil films on surfaces in air flow, with application to the measurement of skin-friction. *J Phys E* 9:3